# A Multi-Channel Passive Brain Implant for Wireless Neuropotential Monitoring

Wei-Chuan Chen, *Student Member, IEEE,* Cedric W. L. Lee, *Student Member, IEEE,*
Asimina Kiourti, *Member, IEEE,* and John L. Volakis, *Fellow, IEEE*

***Abstract*—We propose a novel multi-channel (8 channels) passive neuro-sensing system for wireless acquisition of brain signals as low as 20 $\mu V_{pp}$. Compared to previous batteryless multi-channel neuropotential sensors, the proposed design exhibits: a) 28 times better sensitivity, b) ∼2 times smaller footprint, and c) scalability to 100s or even 1000s of channels. The proposed system consists of an external interrogator and a neuro-recorder implanted inside the scalp. For operation, the interrogator sends a) a 2.4 GHz carrier signal to "turn on" the implant, and b) an infrared control signal for channel selection. The latter activates the desired channel via a photo-activated multiplexer. For this channel, the carrier signal is mixed with the neural signal ($f_{neuro}$) to generate a $4.8\ GHz \pm f_{neuro}$ modulated signal. The latter is then transmitted back to the interrogator. To verify the implant's operation inside biological tissues, $in$-$vitro$ measurements are presented using pig skin. Experimental results show that the proposed neuropotential recorder exhibits 20 $\mu V_{pp}$ sensitivity at all eight channels (viz. it can record any signal generated by the human brain). The system is also in compliance with the strictest Federal Communications Commission standards for patient safety. Notably, the proposed approach is scalable to a much higher number of channels. As such, the proposed system can be a game-changing capability for a wide range of applications.**

***Keywords*—Brain implant, wireless, multichannel, neurosensing, passive, infrared photodiode, photovoltaic cell, antiparallel diode pair, biocompatibility, biomedical telemetry.**

## I. Introduction

DEEP brain neuropotential monitoring can significantly improve the individual's physical and mental well-being. Example applications include: 1) detection and interruption of early epileptic seizures, 2) behavioral studies to determine levels of consciousness, 3) understanding and improving the brain's functionality for patients with Alzheimer's and Parkinson's conditions, among others [1], [2].

Current technology on deep brain neuropotential recording is limited by several factors. Specifically, wires are typically used to connect the implant recorder to external monitoring units [2], [3]. These tethered connections are obtrusive to the patient and restrict long-term brain clinical research in free-moving subjects. To address this concern, wireless brain implants have been pursued. However, current versions of these implants are typically bulky and use batteries or harvesters for powering them [4]. Also, such implants are associated with temperature increases, implying possible damage to the brain tissues or cells [5]. To address these concerns, a batteryless wireless neuropotential recorder was proposed in [6]. However, the recorder still required a battery that was placed external to the skull, limiting comfort, and increasing the risk of infection. Notably, wirelessly powered neural recorders have been reported in [7]–[11], but these still employ complex integrated circuits.

As an alternative, we recently introduced a new class of wireless fully-passive brain implants [13]–[16] that use simple electronic cicuitry. In our latest work [16], we demonstrated a wireless and fully-passive brain implant, but it was used only for single-channel recording. This implanted recorder exhibited a very small footprint of 8.7 mm × 10 mm and was shown to exhibit sensitivity as high as 20 $\mu Vpp$. As such, all signals generated by the human brain, see Table I [12], can be detected. However, the single channel operation of our earlier device [16] is not suited for realistic clinical applications. For the latter, we require 100 or even 1000s of channels of concurrent neuropotential recording.

TABLE I
Voltage And Frequency Range Of Signals Generated By The Human Brain [12]

| Neural Signals | Voltage Range | Frequency Range |
|---|---|---|
| Local field potentials | 20∼ 2000 $\mu V_{pp}$ | 10∼200 Hz |
| Neural spikes | 100 $\mu V_{pp}$ | 300 Hz∼5 kHz |

In this paper, we propose multi-channel neuropotential recording that is wireless and batteryless. Specifically, we design and fabricate a proof-of-concept wireless multi-channel neuropotential monitoring system with the following unique features:

1) wireless, passive and biocompatible operation,

2) concurrent recording from 8 channels by using an infrared transceiver/receiver, scalable to 100s and up to 1000s of channels,

3) neuropotential detection as low as 20 $\mu V_{pp}$ per channel,

4) validation using fresh pig skin to emulate the human skin's properties at RF and infrared bands,

5) extremely small power consumption (98 $\mu W$),

6) compliance with the strictest Federal Communications Commission (FCC) standards for patient safety [17].

W. Chen, C. W. L. Cedric, and A. Kiourti are with the ElectroScience Laboratory, Department of Electrical and Computer Engineering, The Ohio State University, Columbus, OH 43212 USA(e-mail: chen.5825@osu.edu; lee.6256@osu.edu;kiourti.1@osu.edu;)

J. L. Volakis is with the College of Engineering and Computing at Florida International University, Miami, FL 33174 USA (e-mail: jvolakis@fiu.edu)

This work was supported by the National Science Foundation under Grant 1763350

As compared to previous batteryless multi-channel neuropotential recordings [18], the proposed implant exhibits: a) 28 times higher sensitivity, b) ∼2 times smaller footprint (1600 $mm^2$ vs 3000 $mm^2$ in [18]), c) higher scalability (3 photodiodes for 8 channels vs. 8 photodiodes for 8 channels in [18]), and d) alternative and, likely, more practical implementation (using infrared instead of visible light as in [18] for improved skin penertration).

Unfortunately, the design in [16] refers to a single channel and is not scalable for the realistic requirements of 100s and 1000s channel recordings. These multi-channel recordings are needed to understand movement of multiple muscles and study how chronic issues such as Parkinson's and Alzheimer's affect brain functionality.

A number of innovations are brought forward to achieve the proposed scalable multi-channel capabilities, including:
1) use of an infrared exterior transceiver and implanted receiver,
2) integration of an implanted multiplexer,
3) re-design/optimization of the implanted and interrogator antennas for optimal coupling to the new implanted multiplexing unit,
4) re-design/optimization of the entire brain implant and exterior interrogator to accommodate these new features, and
5) use of actual pig-skin, rather than a tissue-emulating phantom, to achieve the desired performance at optical frequencies.

## II. NEUROSENSING SYSTEM OVERVIEW

The block diagram of the proposed neuropotential transceiver and receiver is depicted in Fig. 1. The set-up consists of 1) an implanted recorder placed just under the scalp with the recording electrodes protruding through the bone into the brain, and 2) an external interrogator placed outside the scalp. This operation of the proposed neurosensor involves two processes: 1) wireless monitoring of the neural signal using a process similar to RFIDs, 2) selection/toggle of the different channels via an infrared-enabled implanted multiplexer.

The process for wireless and batteryless neural signal collection/monitoring can be summarized as follows. First, the interrogator sends a 2.4 GHz carrier signal to "turn on" the implanted recorder. The mixer in the implanted device uses the 2.4 GHz signal to generate a $4.8\ GHz \pm f_{neuro}$ modulated signal that is eventually transmitted back to the interrogator. To obtain low conversion loss and suppress the DC term in the mixing process, an anti-parallel diode pair (ADPD) configuration is employed, as described in [14].

For toggling different channels, an extremely low-power commercial multiplexer (Analog Devices, ADG708) is adopted. Further, to provide power and control to the multiplexer, we employed an implanted infrared receiver and an exterior infrared transceiver as shown in Fig. 2. For this particular multiplexer, each of the 8 channels is selected via an "on-off" scheme that employs 3 implanted photodiodes (Vishay, VEMD2000). These three photodiodes can be individually turned on and off to generate 8 different optical combinations. The optical signal is denoted as $P_0$, $P_1$ and $P_2$ as depicted in Fig. 2. Each of the 8 combinations is then used via the multiplexer to select one of the 8 probes for recording. Notably, generation of this $P_0P_1P_2$ code is done via the external infrared emitters as in Fig. 1 and 2. These emitters also pass their signal through the skin to the photovoltaic cell to introduce a stable DC voltage on the multiplexer of the implant. It is noted that thereby power consumption of the implant is due to the multiplexer operation and the resistance of the photodiodes. But the power consumption of the multiplexer operation can be reduced to trivial level by choosing high-value resistors and high-sensitivity photodiodes. Typically, when the series resistance of the photodiode is R = $1.5M\ \Omega$, see Fig. 2, the power consumption is only $16\ \mu W$ (-18 dBm).

In designing the aforementioned neuropotential monitoring system, the goal is to achieve 20 $\mu V_{pp}$ sensitivity for all channels. This would enable recording of all possible neural signals generated by the human brain as shown in Table I. Typically, the minimum detectable neuropotential signal level can be expressed as [16]:

$$\begin{aligned} &MDS_{neuro}[dBm] \\ &= Receiver \quad Sensitivity[dBm] + L_{sys}[dBm]. \end{aligned} \tag{1}$$

where $L_{sys}$ = overall system loss, and in the above $Receiver \quad Sensitivity$ = minimum detectable signal level by the receiver. For our employed interrogator, the sensitivity is -120 dBm [15]. Thus, to guarantees a minimum detectable signal of 20 $\mu V_{pp}$ (or -90 dBm), $L_{sys} < 30$ dB. The receiver system loss, $L_{sys}$, could be divided into three major components as expressed in (2):

$$L_{sys}[dB] = L_{prop}[dB] + L_{conv}[dB] + L_{match}[dB] \tag{2}$$

In the above, $L_{prop}$ = propagation loss between the implanted and the interrogator antenna at $4.8\ GHz \pm f_{neuro}$, $L_{conv}$ = conversion loss at the implanted mixer, and $L_{match}$ = impedance mismatch losses between the antenna and the mixer in the implanted device. To ensure $L_{sys} < 30$ dB, $L_{prop}$, $L_{conv}$ and $L_{match}$ should be minimized to the extent possible. This is discussed in Section III.

Table II compares the proposed multichannel neuropotential monitoring system with previously reported wireless and batteryless neural recorders. The neural recorders in [13]–[16] have only one channel and are therefore not sufficient for realistic clinical applications. A batteryless multichannel system was reported in [18] but this implant has ∼ 2 times larger footprint to achieve 28 times lower sensitivity. Also, in [18], visible light was employed to excite the photodiodes. But visible light cannot penetrate the biological tissues. Further, the design in [18] exhibited limited scalability, requiring 8 photodiodes for 8 channels (rather than 3 photodiodes as done here).

In this paper, we propose the first wireless, passive and scalable fully-implanted device with 20 $\mu V_{pp}$ sensitivity at all channels. Infrared light is used to penetrate through tissues and toggle an N-input multiplexer to activate $2^N$ channels.

For this paper, the focus was totally on the multichannel implant design and demonstrations. Similarly, the implant's

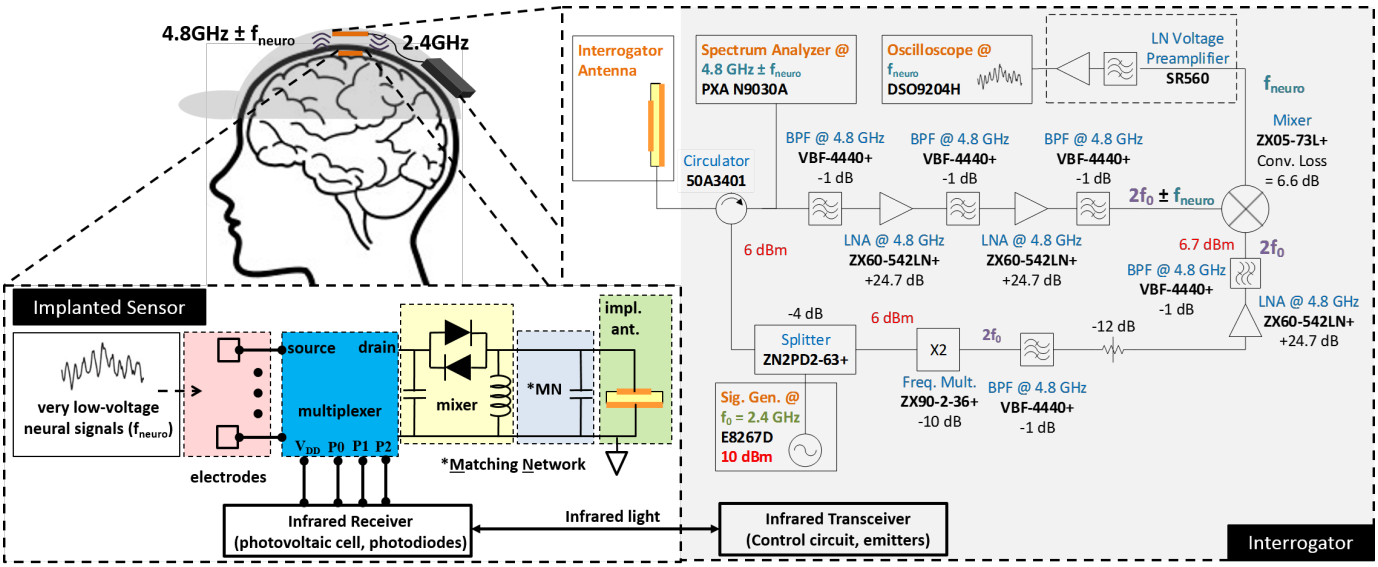


Fig. 1. Block diagram of the proposed mulitchannel neurosensing system.

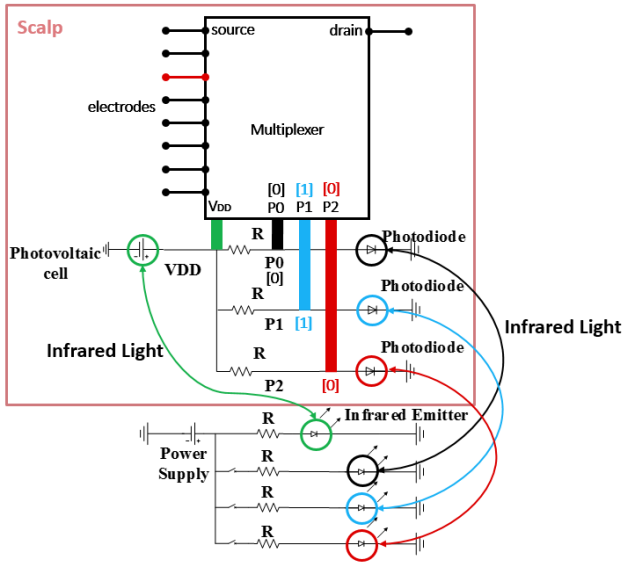


Fig. 2. Proposed implanted infrared receiver and exterior transceiver used to toggle different neuro-channels in a wireless and passive manner. The transceiver employs 3 photodiodes to form a 3 digit code for selecting each of the 8 channels. In this condition, the three digit code is 0,1,0 and channel 3 is selected.

power consumption can be further reduced in the future by using higher-permittivity and lower-loss substrates. The power consumption in Table II shows the average power of all 8 different channel combinations (from 0,0,0 to 1,1,1).

## III. BRAIN IMPLANT AND INTERROGATOR DESIGN

The developed brain implant and interrogator PCB layouts are shown in Fig. 3. For a proof-of-concept demonstration, the implant and interrogator each employed a three-layer metallization structure, occupying a footprint of 40 mm × 40 mm in the area. Specifically, for the implanted neural recorder, the photovoltaic cells and the implanted antenna were placed on the top layer to receive the RF and infrared signals from the interrogator. The multiplexer and mixing circuits were located on the bottom layer. The middle layer contains the common ground shared by the antenna, multiplexer, and the mixing circuits. A similar structure was employed for the interrogator's circuit, as shown in Fig. 3(b). Co-simulations were performed in ANSYS HFSS and Keysight ADS. An in-house genetic algorithm was also employed for design optimization [19]. Below, we discuss the various components that comprise the transceiver.

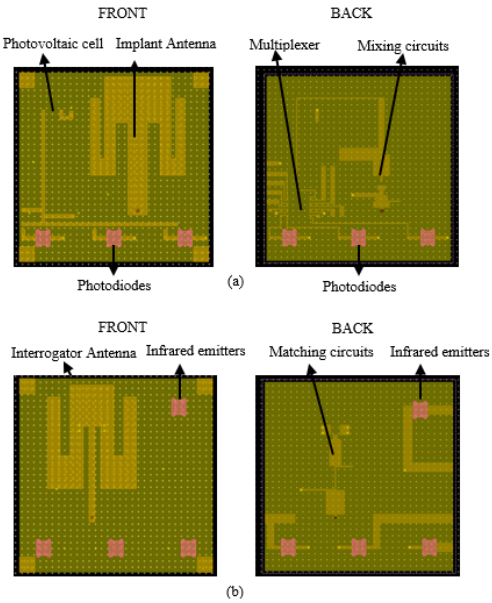


Fig. 3. Proposed system layout: (a) brain implant, and (b) exterior interrogator. The corresponding areas both are 40 mm × 40 mm

TABLE II
COMPARISON BETWEEN PROPOSED VS PREVIOUSLY WIRELESS IMPLANTED DEVICES WITHOUT INTEGRATED CIRCUITS

| Ref | Type | Footprint | Power consumption | Channels | Operation distance | Operation frequency | Min. detectable signal |
|---|---|---|---|---|---|---|---|
| [13] | Implanted | $12 \times 4\ mm^2$ | N/A | 1 | $< 1.5\ cm$ | 2.4 GHz and 4.8 GHz | $3.4m\ V_{pp}$ (in-vitro) |
| [14] | Implanted | $39 \times 15\ mm^2$ | 0.008 mW | 1 | 8 mm | 2.4 GHz and 4.8 GHz | $200\ \mu V_{pp}$ (in-vitro) |
| [15] | Implanted | $16 \times 15\ mm^2$ | 0.035 mW | 1 | $\sim 1.5\ cm$ | 2.4 GHz and 4.8 GHz | $63\ \mu V_{pp}$ (in-vitro) |
| [16] | Implanted | $8.7 \times 10\ mm^2$ | 0.305 mW | 1 | 2 mm | 2.4 GHz and 4.8 GHz | $20\ \mu V_{pp}$ (in-vitro) |
| [18] | Implanted | $\sim 50 \times 60\ mm^2$ | N/A | 3 | 3 mm | 2.45 GHz and 4. 9GHz | $700\ \mu V_{pp}$ (in-vitro) |
| Proposed | Implanted | $40 \times 40\ mm^2$ | 0.598 mW | 8 | 2.5 mm | 2.4 GHz and 4.8 GHz | $20\ \mu V_{pp}$ (in-vitro) |

### A. Implanted and Interrogator Antennas

The implants in [13] and [15] were designed to operate under the skull, while the implants in [16] and this work are intended for operation under the skin. Our target distance of 2.5 mm was selected according to the thickness of the pig-skin used in this experiments. This aligns well with real-life applications, where the thickness of the human head skin ranges from 2 mm to 4 mm, according to age [20]. In this paper, the implanted and interrogator antennas have been optimized for the aforementioned 2.5mm distance.

The implanted and interrogator antennas were designed to overcome propagation loss at 2.4 GHz and $4.8\ GHz \pm f_{neuro}$ and ensure FCC regulations [17]. To achieve dual band radiation, an E-shaped patch antenna geometry was adopted for the implanted and interrogator antennas, shown in Fig. 3. The simulated transmission coefficient $|S_{21}|$ between the implanted and interrogator antennas as a function of the depth into the skin tissue is given in Fig. 4. As seen, $|S_{21}| = -6dB|-14dB$ at 2.4 GHz|4.8 GHz when the implant is 1 mm below the skin. Notably, our interrogator/implanted antenna pair is designed and optimized in the reactive near-field mode. Because of the poor antenna gain in the far-field mode, any unintended 2.4 GHz signal is precluded from reaching the implant. Even if a strong interference 2.4 GHz signal was present, the power would not be sufficient to activate the brain implant given the poor antenna gain and tissue loss.

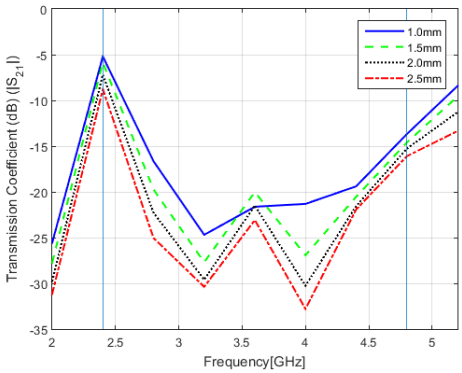


Fig. 4. Simulated transmission coefficient, $|S_{21}|$, between the transmitting and receiving antennas for different pig skin depth.

### B. Implant Mixer

The goal of the mixer design is to decrease the conversion and mismatch losses ($L_{conv}$ and $L_{match}$) mentioned in Section II. The employed mixer consists of the following:

1) Antiparallel Diode Pair (APDP),

2) Inductor that provides the circuit's route to ground for the low-frequency neuropotential signal ($f_{neuro}$),

3) Capacitor that acts as short for the 2.4GHz to isolate the DC from the neuropotential signal ($f_{neuro}$),

4) Matching circuit to minimize mismatch losses between the antenna (50 Ω) and mixer. To further reduce the number of lumped elements, the inductor and capacitor were replaced by short- and open-circuited transmission lines, respectively. The final mixer and matching circuit PCB layout is shown in Fig. 3(a). It is noted that commercial APDP diodes (Avago Technologies, HSMS-286C) with good circuit balance were employed for subharmonic mixing.

### C. Infrared Transceiver/Receiver

The infrared exterior transceiver and implanted receiver are intended to provide 1) stable DC voltage of 3V, and 2) a control signal to the implanted multiplexer for toggling among the different channels. To ensure batteryless operation, the DC voltage is provided via an infrared-illuminated photovoltaic cell. The control signal is provided by the 3 digit code generated by the photodiodes. It is important that the infrared receiver have sufficient isolation to ensure detection of the 3 digit code. Otherwise, the infrared emitter can lead to erroneous channel turn on. To avoid this, highly directive photodiodes and photoemitters were selected (The patterns of the photodiodes are given in Fig. 5(a) and 5(b)).

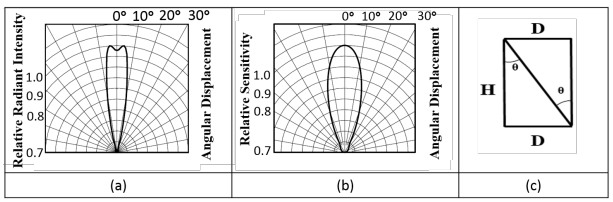


Fig. 5. Radiation and reception pattern for the (a) infrared emitter, (b) photodiodes and (c) the geometry of the photodiodes and photo emitters

As seen in Fig. 5, the radiation receiving sensitivity at 20° from the normal intensity is rather low. This ensures excellent isolation between the adjacent photodiodes. The suggested separation between two photodiodes should be:

$$D = H \cdot tan\theta \tag{3}$$

where H = thickness of the skin, and $\theta$ = infrared beam angle between the photodiode and the neighboring emitter. Typically, $5\ mm < H < 8\ mm$ and $\theta < 20°$. Based on these averages, the distance between the photodiodes should be at least $D \approx 2\ mm$. That is, the goal isolation between different channels can be achieved by the designated physical placement of the photodiodes.

### D. RF Interrogator

The RF interrogator is intended to: a) generate and receive the backscattered $4.8\ GHz \pm f_{neuro}$ after third-order mixing, and b) demodulate the mixing product and display/store the recovered time domain signal. As would be expected, demodulation can be performed by mixing the backscattered signal with another 4.8 GHz reference signal to obtain the "baseband" neuropotential at $f_{neuro}$.

The employed interrogator system is displayed in Fig. 1 and a similar version was used in [16]. For the set up in Fig. 1, multiple stages of filtering and amplification were used to improve the signal to noise ratio. Notably, this architecture has a very low noise figure of 3.8 dB.

## IV. NEUROSENSING SYSTEM PERFORMANCE

### A. Fabricated Prototype

The fabricated brain implant and interrogator propotypes are shown in Fig. 6. As mentioned earlier, for this proof-of-concept demonstration, both devices occupy a footprint of 40 mm $\times$ 40 mm. They were fabricated on Rogers RO4003C substrate ($\epsilon_r = 3.38$, $tan\delta = 0.0021$) of thickness 40 mils (1.016 mm). To ensure biocompatibility, the implanted recorder was coated with a 0.7 mm-thick layer of Polydimethylsiloxane ($\epsilon_r = 2.8$, $tan\delta = 0.001$ [15]). This relatively lossless layer decreases the power absorbed by the human tissue, thereby reducing losses between the implant and interrogator antennas [21].

Selection of a higher permittivity substrate will further miniaturize the implant by shrinking the antenna and microstrip feed lines. We have already identified high permittivity materials (TMM 13i, $\epsilon_r = 12.2$, $tan\delta = 0.0019$) that exhibit the similar loss tangent to the low permittivity dielectric employed in this work (RO4003C, $\epsilon_r = 3.38$, $tan\delta = 0.0021$). We have also identified flexible polymer-ceramic composites having $tan\delta \approx 0.0025$ for $\epsilon_r \approx 10$ [22]. That is, we are confident that we can switch to higher-permittivity dielectrics without increasing dielectric losses.

### B. Measurement Setup

The measurement setup used to validate the 20 $\mu V_{pp}$ sensitivity of our neuropotential detector for all channels is shown in Fig. 7. As depicted, the 2.4 GHz carrier was a pure 6 dBm sinusoid that was supplied to the interrogator using a signal generator (Agilent SG386). Also, the emulated neuropotentials at $f_{neuro} = 10$ Hz to 5 kHz were generated using an arbitrary function generator (Leader, LFG-1300). For the infrared control circuit, shown in Fig. 6, manual turn on/off switches were used. To emulate the human head

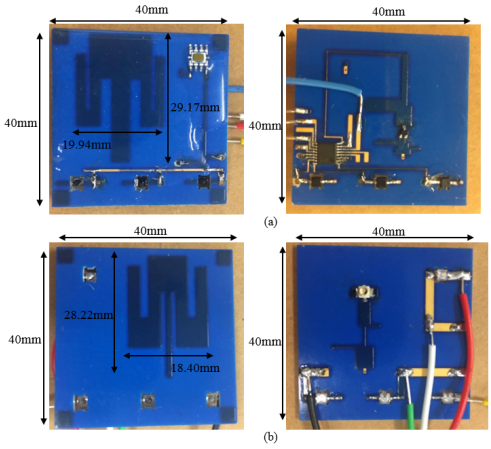


Fig. 6. Fabricated prototypes: (a) brain implant, (b) exterior interrogator

tissues, the neural recorder was immersed inside a four-layer head phantom shown in Fig. 6. For this phantom, the bone, dura/gray matter, and white matter tissues were formulated using the recipes in [23]. For the skin, we used fresh pig skin layer [24]. Conventional phantoms accurately emulate the dielectric properties of human tissues, but not their light penetration properties. With this in mind, pig skin (viz. actual biological tissue) is selected as to better emulate both RF and infrared signal propagation. The permittivity and loss tangent of the pig-skin were measured using the Agilent 85070E Dielectric Probe Kit and further compared vs. the theoretical skin properties [25] shown in Fig. 8. The reader is referred to [26]–[28] for infrared losses through the scalp.

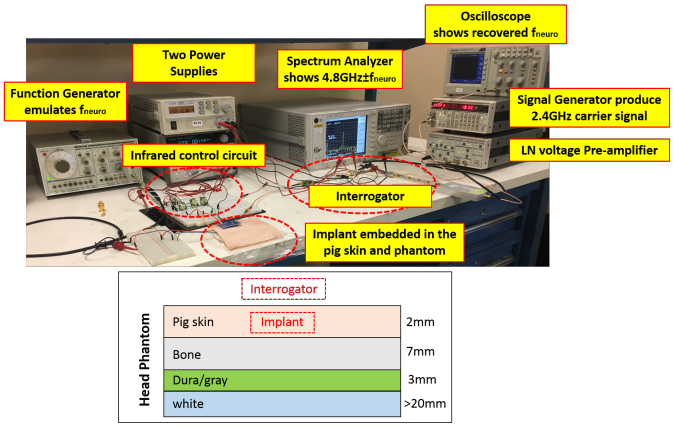


Fig. 7. The neurosensing measurement setup with the layered head phantom.

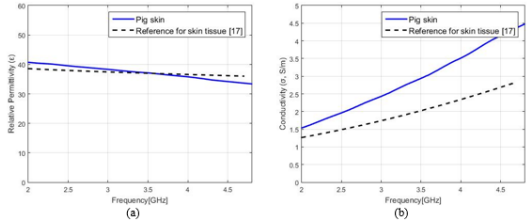


Fig. 8. (a) Measured permittivity, and (b) measured conductivity of pig-skin versus the reference skin properties reported in [25].

### C. Minimum detectable signal

As already noted, our goal is to detect neural signals down to 20 $\mu V_{pp}$. To achieve this, we must minimize the overall losses between the interrogator and implant. This overall system loss, $L_{sys}$, is defined as the difference between the power of the neuropotential signals detected at the input of the implanted device ($f_{neuro}$) and the backscattered power received at the interrogator ($4.8\ GHz \pm f_{neuro}$). Based on simulations, we found that $L_{sys}$ = -18.2 dB when 10 Hz $< f_{neuro} <$ 5 kHz for a distance of 2.5 mm between the implant and interrogator. Our measurements using a pig skin thickness of 2.0 mm indicated that $L_{sys}$ = -25 dB. Although $L_{sys}$ is 7 dB larger than simulation, it still meets the system loss criteria of $L_{sys} < 30$ dB. Fig. 9 shows example demodulated backscattered signals received at the interrogator. For these example waveforms, the emulated neuropotentials were as low as 20 $\mu V_{pp}$. The observed higher noise can be attributed to the preamplifier filter used at the interrogator. This noise can be suppressed by using filters.

| $f_{neuro}$ (Hz) | $f_L$ and $f_H$ (HZ) | Recovered Waveform | $f_{neuro}$ (Hz) | $f_L$ and $f_H$ (HZ) | Recovered Waveform |
|---|---|---|---|---|---|
| 10 | 1-10 | 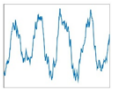 | 500 | 300-1000 | 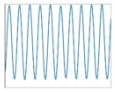 |
| 50 | 10-300 |  | 1000 | 300-1000 | 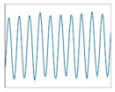 |
| 100 | 10-300 | 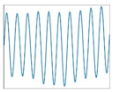 | 5000 | 3K-10K | 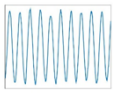 |

Fig. 9. Time-domain performance for minimum detectable neural signal ($MDS_{neuro}$ = 20 $\mu V_{pp}$)

### D. Specific Absorption Rate (SAR)

To confirm that the proposed neurosensing system meets the FCC safety guidelines, a 10-cm-radius spherical head model was employed. This model was composed of skin (9.2-cm-radius), bone (8.5-cm-radius), gray matter (7.8-cm-radius), and white matter (7.5-cm-radius) tissues [29]. The implant was placed in the middle of the skin layer.

For SAR simulation, the brain implant was placed below the skin layer and the interrogator was placed right above it. It was found that the average SAR for 1 g of tissue with 6 dBm carrier power at 2.4 GHz had a max value of $SAR_{1g}$ = 0.368 W/kg. This value conforms to the strictest FCC requirements of $SAR_{1g} < 1.6$ W/kg for uncontrolled environment exposure [17].

## V. CONCLUSION

A multichannel passive neurosensing system was proposed for the wireless acquisition of deep brain signals as low as 20 $\mu V_{pp}$. This multichannel neurosensors employed an implanted multiplexer and an infrared transceiver/receiver module. An 8-channel prototype was designed and demonstrated to achieve 20 $\mu V_{pp}$ sensitivity in all channels under $in-vitro$ conditions.

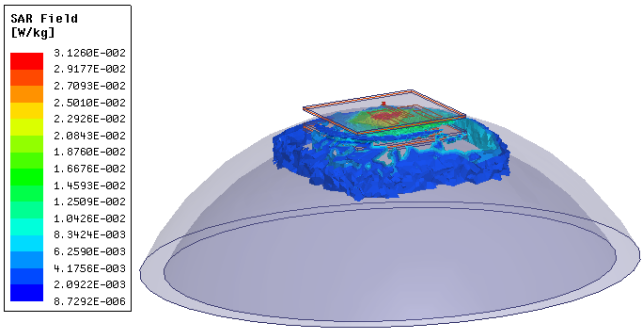


Fig. 10. SAR performance averaged over 1 g with input carrier power at 2.4 GHz and 6 dBm.

That is, most neural signals generated by the human brain can be detected across all 8 channels in a passive and wireless manner. This is a game-changing capability for a very wide range of applications.

Future work will target three major directions:

1) $In$-$vivo$ testing. The ultimate goal of the wireless passive implanted system is to record neuropotentials $in-vivo$. In the past, we successfully recovered ECG (Electrocardiography) signals from the human body using commercial electrodes attached to our device. Future studies will explore brain signal acquisition from animals. We note that $in$-$vivo$ data are expected to be noisier (e.g., motion artifacts or noise from other equipment) and can be possibly corrupted by 50/60 Hz signals associated from power lines in the operation room. In this case, notch filtering will be required to remove the 50/60 Hz interference, and more sophisticated signal processing techniques may be needed to retrieve the neural signals (e.g., window averaging).

2) System miniaturization. For our proof-of-concept multi-channel board reported in this work, the footprint of the circuit is relatively large ($40\ mm \times 40\ mm$). The largest portion of the circuit area is occupied by the implanted antenna. Therefore antenna miniaturization will be explored by: 1) choosing higher dielectric constant substrates, and 2) employing more sophisticated antenna designs.

3) Channel scalability. In our proposed system, channel scalability is achieved by using N photodiodes for $2^N$ channels. For the 8-channel system reported in this work, 3 photodiodes are employed. Using 10 photodiodes, we can reach $2^{10}$ = 1024 channels. To maintain a small implant size, customized photodiodes and multiplexers would also be required. The former implies frequency-dependent photodiodes that use both frequency and physical separation to reduce total footprint. We would also require miniature in-house multiplexer designs. Higher permittivity materials can be employed to reduce the antenna footprint and microstrip line size. In terms of power consumption, if the photodiode serial resistance is kept high ($M\Omega$ level, per Section II of the manuscript), it is predicted that the estimated power consumption by a 10-photodiode layout will be similar to that of the 3-photodiode layout reported in this work.

## REFERENCES

[1] G. Schalk and E. C. Leuthardt, "Brain-computer interfaces using electrocorticographic signals," *IEEE Reviews in Biomedical Engineering*, vol. 4, pp. 140–154, 2011.

[2] K. D. Wise, A. M. Sodagar, Y. Yao, M. N. Gulari, G. E. Perlin, and K. Najafi, "Microelectrodes, microelectronics, and implantable neural microsystems," *Proceedings of the IEEE*, vol. 96, no. 7, pp. 1184–1202, July 2008.

[3] A. Waziri, C. A. Schevon, J. Cappell, R. G. Emerson, G. M. McKhann, II, and R. R. Goodman, "Initial surgical experience with a dense cortical microarray in epileptic patients undergoing craniotomy for subdural electrode implantation," *Neurosurgery*, vol. 64, no. 3, pp. 540–545, 2009.

[4] E. Moradi, T. Bjrninen, L. Sydnheimo, J. M. Carmena, J. M. Rabaey, and L. Ukkonen, "Measurement of wireless link for brainmachine interface systems using human-head equivalent liquid," *IEEE Antennas and Wireless Propagation Letters*, vol. 12, pp. 1307–1310, 2013.

[5] S. Kim, P. Tathireddy, R. A. Normann, and F. Solzbacher, "Thermal impact of an active 3-d microelectrode array implanted in the brain," *IEEE Transactions on Neural Systems and Rehabilitation Engineering*, vol. 15, no. 4, pp. 493–501, Dec 2007.

[6] M. Yin, D. A. Borton, J. Komar, N. Agha, Y. Lu, H. Li, J. Laurens, Y. Lang, Q. Li, C. Bull *et al.*, "Wireless neurosensor for full-spectrum electrophysiology recordings during free behavior," *Neuron*, vol. 84, no. 6, pp. 1170–1182, 2014.

[7] L. Song and Y. Rahmat-Samii, "An end-to-end implanted brain–machine interface antenna system performance characterizations and development," *IEEE Transactions on Antennas and Propagation*, vol. 65, no. 7, pp. 3399–3408, 2017.

[8] E. Moradi, S. Amendola, T. Björninen, L. Sydänheimo, J. M. Carmena, J. M. Rabaey, and L. Ukkonen, "Backscattering neural tags for wireless brain-machine interface systems," *IEEE Transactions on Antennas and Propagation*, vol. 63, no. 2, pp. 719–726, 2015.

[9] S. Stoecklin, A. Yousaf, T. Volk, and L. M. Reindl, "Efficient wireless powering of biomedical sensor systems for multichannel brain implants." *IEEE Trans. Instrumentation and Measurement*, vol. 65, no. 4, pp. 754–764, 2016.

[10] R. Muller, H.-P. Le, W. Li, P. Ledochowitsch, S. Gambini, T. Bjorninen, A. Koralek, J. M. Carmena, M. M. Maharbiz, E. Alon *et al.*, "A minimally invasive 64-channel wireless $\mu$ecog implant," *IEEE Journal of Solid-State Circuits*, vol. 50, no. 1, pp. 344–359, 2015.

[11] H. Ando, K. Takizawa, T. Yoshida, K. Matsushita, M. Hirata, and T. Suzuki, "Wireless multichannel neural recording with a 128-mbps uwb transmitter for an implantable brain-machine interfaces," *IEEE transactions on biomedical circuits and systems*, vol. 10, no. 6, pp. 1068–1078, 2016.

[12] R. R. Harrison, "The design of integrated circuits to observe brain activity," *Proceedings of the IEEE*, vol. 96, no. 7, pp. 1203–1216, 2008.

[13] H. N. Schwerdt, W. Xu, S. Shekhar, A. Abbaspour-Tamijani, B. C. Towe, F. A. Miranda, and J. Chae, "A fully passive wireless microsystem for recording of neuropotentials using rf backscattering methods," *Journal of Microelectromechanical Systems*, vol. 20, no. 5, pp. 1119–1130, 2011.

[14] C. W. Lee, A. Kiourti, J. Chae, and J. L. Volakis, "A high-sensitivity fully passive neurosensing system for wireless brain signal monitoring," *IEEE Transactions on Microwave Theory and Techniques*, vol. 63, no. 6, pp. 2060–2068, 2015.

[15] A. Kiourti, C. W. Lee, J. Chae, and J. L. Volakis, "A wireless fully passive neural recording device for unobtrusive neuropotential monitoring." *IEEE Trans. Biomed. Engineering*, vol. 63, no. 1, pp. 131–137, 2016.

[16] C. W. Lee, A. Kiourti, and J. L. Volakis, "Miniaturized fully passive brain implant for wireless neuropotential acquisition," *IEEE Antennas and Wireless Propagation Letters*, vol. 16, pp. 645–648, 2017.

[17] U. F. C. Commission *et al.*, "Report and order fcc 96–326," 1996.

[18] H. N. Schwerdt, F. A. Miranda, and J. Chae, "Wireless fully passive multichannel recording of neuropotentials using photo-activated rf backscattering methods," *IEEE Transactions on Microwave Theory and Techniques*, vol. 63, no. 9, pp. 2965–2970, 2015.

[19] R. L. Haupt and D. H. Werner, *Genetic algorithms in electromagnetics*. John Wiley & Sons, 2007.

[20] H. Hori, G. Moretti, A. Rebora, and F. Crovato, "The thickness of human scalp: normal and bald," *Journal of Investigative Dermatology*, vol. 58, no. 6, pp. 396–399, 1972.

[21] F. Merli, B. Fuchs, J. R. Mosig, and A. K. Skrivervik, "The effect of insulating layers on the performance of implanted antennas," *IEEE Transactions on Antennas and propagation*, vol. 59, no. 1, pp. 21–31, 2011.

[22] S. Koulouridis, G. Kiziltas, Y. Zhou, D. J. Hansford, and J. L. Volakis, "Polymer–ceramic composites for microwave applications: fabrication and performance assessment," *IEEE Transactions on Microwave Theory and Techniques*, vol. 54, no. 12, pp. 4202–4208, 2006.

[23] K. Ito, K. Furuya, Y. Okano, and L. Hamada, "Development and characteristics of a biological tissue-equivalent phantom for microwaves," *Electronics and Communications in Japan (Part I: Communications)*, vol. 84, no. 4, pp. 67–77, 2001.

[24] T. Karacolak, R. Cooper, E. S. Unlu, and E. Topsakal, "Dielectric properties of porcine skin tissue and in vivo testing of implantable antennas using pigs as model animals," *IEEE Antennas and Wireless Propagation Letters*, vol. 11, pp. 1686–1689, 2012.

[25] S. Gabriel, R. Lau, and C. Gabriel, "The dielectric properties of biological tissues: Ii. measurements in the frequency range 10 hz to 20 ghz," *Physics in medicine & biology*, vol. 41, no. 11, p. 2251, 1996.

[26] A. Young, T. Germon, N. Barnett, A. Manara, and R. Nelson, "Behaviour of near-infrared light in the adult human head: implications for clinical near-infrared spectroscopy." *British journal of anaesthesia*, vol. 84, no. 1, pp. 38–42, 2000.

[27] A. N. Bashkatov, E. A. Genina, V. I. Kochubey, and V. V. Tuchin, "Optical properties of human cranial bone in the spectral range from 800 to 2000 nm," in *Saratov Fall Meeting 2005: Optical Technologies in Biophysics and Medicine VII*, vol. 6163. International Society for Optics and Photonics, 2006, p. 616310.

[28] A. Bashkatov, E. Genina, V. Kochubey, and V. Tuchin, "Optical properties of human skin, subcutaneous and mucous tissues in the wavelength range from 400 to 2000 nm," *Journal of Physics D: Applied Physics*, vol. 38, no. 15, p. 2543, 2005.

[29] J. Kim and Y. Rahmat-Samii, "Implanted antennas inside a human body: Simulations, designs, and characterizations," *IEEE Transactions on microwave theory and techniques*, vol. 52, no. 8, pp. 1934–1943, 2004.

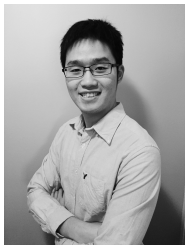

**Wei-Chuan Chen** (S17) received the B.S. degree in electrical engineering from the National Taiwan University, Taipei, Taiwan in 2014. He is currently working toward the Ph.D. degree at The Ohio State University, Columbus OH, USA from 2015.

His research interests include antenna design, computational electromagnetic, RF/microwave circuit and its applications in medical.

**Cedric W. L. Lee** (S13) received the B.S. (First Class Hons.) and M.Sc. degrees in electrical engineering from the National University of Singapore, Singapore, in 2010 and 2013, respectively.

He is currently working toward the Ph.D. degree at The Ohio State University, Columbus OH, USA. He is also a Member of Technical Staff with the DSO National Laboratories, Singapore, where he was involved with the design of antennas prior to his Ph.D. studies. His research interests include RF/microwave circuit and antenna design for radar, wireless communication systems, and medical applications.

Mr. Lee received the Best Student Paper Award at the IEEE International Microwave Workshop Series on RF and Wireless Technologies for Biomedical and Healthcare Applications in 2014.

**AsiminaKiourti** (S10–M14) received the Diploma degree in electrical and computer engineering from the University of Patras, Patras, Greece, in 2008, the M.Sc. degree in technologies for broadband communications from University College London, London, U.K., in 2009, and the Ph.D. degree in electrical and computer engineering from the National Technical University of Athens, Athens, Greece, in 2013.

Dr. Kiourti is currently an Assistant Professor of Electrical and Computer Engineering at The Ohio State University and the ElectroScience Laboratory, Columbus, OH, USA. From 2013 to 2016 she served as a Post-Doctoral Researcher and then a Senior Research Associate at the ElectroScience Laboratory. During her career, she has (co-)authored over 35 journal papers, 80 conference papers, and 7 book chapters. Her research interests include wearable and implantable sensors, antennas and electromagnetics for body area applications, and flexible textile-based electronics.

Dr. Kiourti has received several awards and scholarships, including the IEEE Engineering inMedicine and Biology Society (EMB-S) Young Investigator Award for 2014, the IEEE Microwave Theory and Techniques Society (MTTS) Graduate Fellowship for Medical Applications for 2012, and the IEEE Antennas and Propagation Society (AP-S) Doctoral Research Award for 2011. She is currently serving as an Associate Editor for the IEEE Transactions on Antennas and Propagation.

**John L. Volakis** (S77–M82–SM89–F96) was born on May 13, 1956 in Chios, Greece and immigrated to the U.S.A. in 1973. He obtained his B.E. Degree, summa cum laude, in 1978 from Youngstown State Univ., Youngstown, Ohio, M.Sc. in 1979 from The Ohio State Univ., Columbus, Ohio and the Ph.D. degree in 1982, also from the Ohio State Univ.

Prof. Volakis started his career at Rockwell International (1982-84), now Boeing. In 1984, he was appointed Assistant Professor at The University of Michigan, Ann Arbor, MI, becoming a full Professor in 1994. He also served as the Director of the Radiation Laboratory from 1998 to 2000. From January 2003 to Aug 2017 he was the Roy and Lois Chope Chair Professor of Engineering at the Ohio State University, Columbus, Ohio and served as the Director of the ElectroScience Laboratory from 2003 to 2016. Effective August 2017 he is the Dean of the College of Engineering and Computing and a Professor in the Electrical and Computer Engineering at Florida International University (FIU).

Over the years, he carried out research in antennas, wireless communications and propagation, computational methods, electromagnetic compatibility and interference, design optimization, RF materials, multi-physics engineering, millimeter waves, terahertz and medical sensing. His publications include 8 books, 400 journal papers, nearly 800 conference papers, 26 book chapters and 17 patents/patent disclosures. Among his co-authored books are: Approximate Boundary Conditions in Electromagnetics, 1995; Finite Element Methods for Electromagnetics, 1998; 4th edition Antenna Engineering Handbook, 2007; Small Antennas, 2010; and Integral Equation Methods for Electromagnetics, 2011). He has graduated/mentored nearly 90 doctoral students/post-docs with 41 of them receiving best paper awards at conferences. His service to Professional Societies include: 2004 President of the IEEE Antennas and Propagation Society (2004), Chair of USNC/URSI Commission B (2015-2017), twice the general Chair of the IEEE Antennas and Propagation Symposium, IEEE APS Distinguished Lecturer, IEEE APS Fellows Committee Chair, IEEE-wide Fellows committee member and Associate Editor of several journals. He was listed by ISI among the top 250 most referenced authors (2004), and is a Fellow of IEEE and ACES. Among his awards are: The Univ. of Michigan College of Engineering Research Excellence award (1993), Scott award from The Ohio State Univ. College of Engineering for Outstanding Academic Achievement (2011), IEEE AP Society C-T. Tai Teaching Excellence award (2011), IEEE Henning Mentoring award (2013), IEEE Antennas and Propagation Distinguished Achievement award (2014), The Ohio State University Distinguished Scholar Award (2016), and The Ohio State Univ. ElectroScience George Sinclair Award (2017). He is a Fellow of the Applied Computational Electromagnetics Society.